Structural and Ordering Behavior of Lamellar Polystyrene-*block*-Polybutadiene-*block*-polystyrene Triblock Copolymer Containing Layered Silicates

A. Vazquez,[1] M. López,[1] E. Serrano,[1] A. Valea,[3] N. E. Zafeiropoulos,[2] I. Mondragon[1]

[1]*"Materials + Technologies" Group. Dpto. Ingeniería Química y M. Ambiente, Escuela Politécnica, Universidad País Vasco/Euskal Herriko Unibertsitatea. Pza. Europa 1. 20018 Donostia/San Sebastián, Spain*
[2]*Leibniz Institute of Polymer Research Dresden. Department of Nanomaterials, Hohe Strasse 6, 01069 Dresden, Germany*
[3]*E.U. Ingeniería Técnica Industrial de Bilbao. Ingeniería Química y del Medio Ambiente. Plaza La Casilla, 3, Bilbao, Spain*

Received 5 December 2007; accepted 9 June 2008
DOI 10.1002/app.28885
Published online 17 September 2008 in Wiley InterScience (www.interscience.wiley.com).

ABSTRACT: Nanocomposites based on organically modified montmorillonites (OMMTs) and sodium montmorillonite (CLO-Na^+) with poly(styrene-*b*-butadiene-*b*-styrene) (SBS) diblock copolymer have been investigated. Solution blending of OMMT suspension in toluene with SBS and subsequent static casting and annealing resulted in transparent films. Final samples were processed by compression molding. The intercalation spacing in the nanocomposites, microphase separation of the SBS, and the degree of dispersion of nanocomposites were investigated by X-ray diffraction (Wide and small-angle X-ray scattering), transmission optical microscopy (TOM), atomic force microscopy (AFM), and transmission electron microscopy (TEM). The increase of basal spacing of OMMT in the nanocomposites suggested the intercalation of SBS. The lamellar structure perfection was extensively affected by both OMMT. AFM images and TOM micrographs only showed well dispersed but not exfoliated nanocomposites. On the other hand, TEM showed inserted tactoids into both blocks depending on the surfactant used (stained samples) and the dispersion of those tactoids (unstained samples). Fourier transform infrared spectroscopy indicated only the presence of the OMMT into the SBS. Deviations of the decomposition pathway of pristine SBS with addition of the OMMT were found by thermogravimetric analysis. © 2008 Wiley Periodicals, Inc. J Appl Polym Sci 110: 3624–3637, 2008

Key words: block copolymers; organo-montmorillonites; nanocomposites; structural characterization

INTRODUCTION

Nanocomposites consisting of layered-silicate montmorillonites in a polymer matrix have attracted considerable technological and scientific interest in recent years due to their outstanding physical and mechanical properties such as strength and stiffness, flame retardance, and gas permeability barrier.[1–3] For example, the dispersion of thin montmorillonite layers based on $[H_3N(CH_2)_{11}COOH]^+$-montmorillonite in a semicrystalline nylon-6 matrix greatly improved the tensile strength, modulus, heat distortion temperature, and gas permeability with respect to pristine nylon 6.[4] Polyimide/montmorillonite hybrid[5] and poly(ε-caprolactone)/ montmorillonite[6] nanocomposites have been used for electronic packaging and also as water barrier membranes. Polyether matrix nanocomposites have also been prepared from the polymerization of an epoxy resin.[7] Polystyrene (PS),[8,9] poly(vinylidine fluoride),[10] poly(ethylene oxide),[11] poly(methyl methacrylate),[12] poly(propylene),[13] and poly(lactide acid)[14] can be directly intercaled in organically modified silicates. Recently, organosilicate layer nanocomposites have been prepared with multicomponent polymers such as polymer blends and block copolymers.[15–19] Block copolymers have received much scientific and technological attention because of their ability to self-assemble into a series of periodic ordered microstructures via microphase separation between the constituent block segments.[20–22] Microphase separation of block copolymers takes place, in most cases upon cooling from the disordered melts, as a result of the increase in unfavorable interactions between segmental block components, which is analogous in thermodynamic nature to the upper critical solution temperature behavior of polymer blends.[23–27]

Correspondence to: I. Mondragon (inaki.mondragon@ehu.es).

Contract grant sponsor: Ministerio de Educación y Ciencia; contract grant number: MAT 2003-08125.
Contract grant sponsor: Basque Government (ETORTEK-NANOTRON project).

© 2008 Wiley Periodicals, Inc.

Wide and small-angle X-ray scattering (WAXS and SAXS), and atomic force microscopy (AFM) studies have been carried out to probe the macroscopic morphological change of the ordered structures of the block copolymers because of the compositional fluctuation near OOT and ODT.[28–31]

Layered organosilicate nanocomposites have also been prepared with block copolymers. Lee et al.[32] in their study of a polystyrene-*b*-poly(ethylene-*co*-butylene)-*b*-polystyrene (SEBS) with 17 wt % PS, having cylindrical–hexagonal morphology, demonstrated that OOT and ODT of the nanocomposite were reduced from 209 to 201°C and from 241 to 230°C, respectively, with the addition of the organo-montmorillonite. When the evolution of the morphological change was investigated by isothermal/isochronal time sweep tests, acceleration of the development of spherical domains was observed. The key factor for producing single montmorillonite layer block copolymer nanocomposites has been to ensure that one of the blocks has a good affinity for the montmorillonite. To get this, Ha et al.[33] used two ways, grafting-from (FC) carried out by initiated styrene polymerization from the montmorillonite surface and grafting-to- montmorillonite (TC) where amino functionalizated PS was used to modify the montmorillonite through cation exchange reaction, getting the first experimental demonstration that dispersed montmorillonite could dictate the global orientation of the block copolymer. As suggested by Zhang et al.,[34] strong interactions existing between organically modified montmorillonites (OMMT) and poly(styrene-*b*-butadiene-*b*-styrene) (SBS) led to an improvement in thermal stability. An intercaled nanocomposite of SBS and OMMT was prepared by a solution approach by Liao et al.[35] X-ray pattern and transmission electron microscopy (TEM) observations indicated swelling of galleries of OMMT by SBS and a randomly dispersion of the MMT layers in SBS matrix. Eventually, Yamaguchi and Yamada,[36] using OMMT with various amounts of stearic acid (SA), demonstrated by WAXS and high-resolution field-emission scanning electron microscopy the effectiveness of OMMT containing SA for the preparation of SBS nanocomposites.

In this study, the influence of the layered organosilicate on self-assembled structures of block copolymer-matrix nanocomposites was investigated. The copolymer, OMMT and nanocomposites were characterized using Fourier transform infrared spectroscopy (FTIR) and thermogravimetric analyses (TGA). The effect of addition of OMMT on the structure of these nanocomposites was investigated by WAXS and SAXS, transmission optical microscopy (TOM), AFM, and TEM.

EXPERIMENTAL SECTION

Materials

The work was carried out with a commercial SBS block copolymer (Kraton® D-4274), with 0.2 wt % antioxidant. The block copolymer used, Kraton D-4274, was a gift from Kraton Polymers. Kraton D-4274 is a branched block copolymer composed of SB block stars, with end blocks of PS and a small percentage of linear SBS triblock copolymer. This copolymer was synthesized by anionic polymerization, using alkyl *litio* as initiator and a coupling agent to get star structure. It has a number–average molecular weight (M_n) of 183,000 refered to PS and a polydispersity index 1.34 (as measured by gel permeation chromatography).[37] According to quantitative ^{1}H NMR (Bruker 500 MHz) spectral analyses, the SBS block copolymer contained 58.5 wt % PS, 37.6 wt % 1,4-polybutadiene and 3.9 wt % 1,2-polybutadiene.[37] Besides, Irganox antioxidant was used in 1 wt % with respect to copolymer to prevent degradation during thermal processing.

Pristine sodium montmorillonite (CLO-Na^+), supplied by Southern Clay Products, Inc., with a cation exchange capacity of 95.1 cmol/kg, as measured by ammonium acetate method,[38] was used. The modifiers were ammonium chloride and bromide salts with aliphatic tails and benzyl-aliphatic tails surfactants supplied by Sigma-Aldrich. The surfactants were dioctadecyl dimethylammonium bromide (DMOcA) and hexadecyl benzyl dimethylammonium chloride (BDHA). The choice of the surfactant used in these nanocomposites was done by analysis of solubility parameters (SPs) of surfactants and blocks of the copolymers. The calculated SP using Hoftyzer and Van Krevelen molar attraction constants[39] for the blocks and surfactants are shown in Table I. DMOcA surfactant was expected to have more affinity with butadiene and BDHA with styrene block.

Montmorillonite modification procedure

Modification of pristine montmorillonite (CLO-Na^+) was performed into organo-montmorillonite by cation exchange reaction with surfactant salts.[40–43] A

TABLE I
Calculated Solubility Parameters (SP) of Polymer and Surfactants Using Molar Attraction Constants of Hoftyzer and Van Krevelen [39]

Sample	SP ($J^{1/2}/cm^{3/2}$)
Poly(styrene)-block	17.5
Poly(butadiene)-block	16.9
Dioctadecyl dimethylammonium	16.1
Hexadecyl benzyl dimethylammonium	17.9

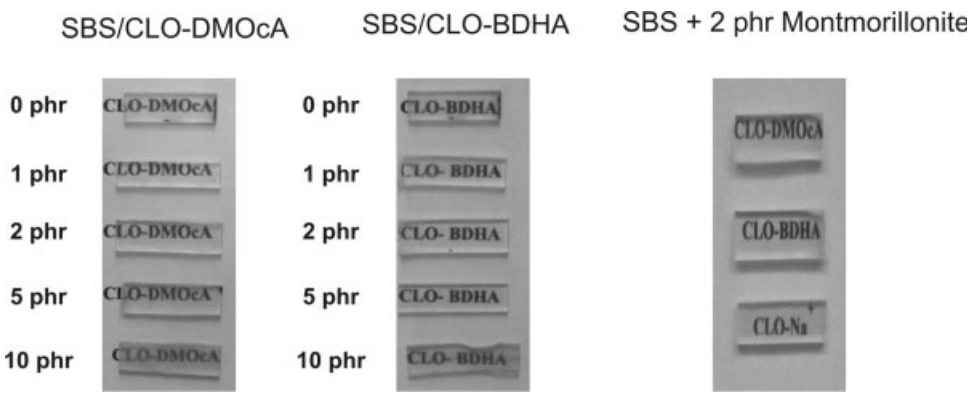

Figure 1 Relative variation of transparency of nanocomposites films with several CLO-DMOcA and CLO-BDHA contents and nanocomposite with 2 phr CLO-Na^+.

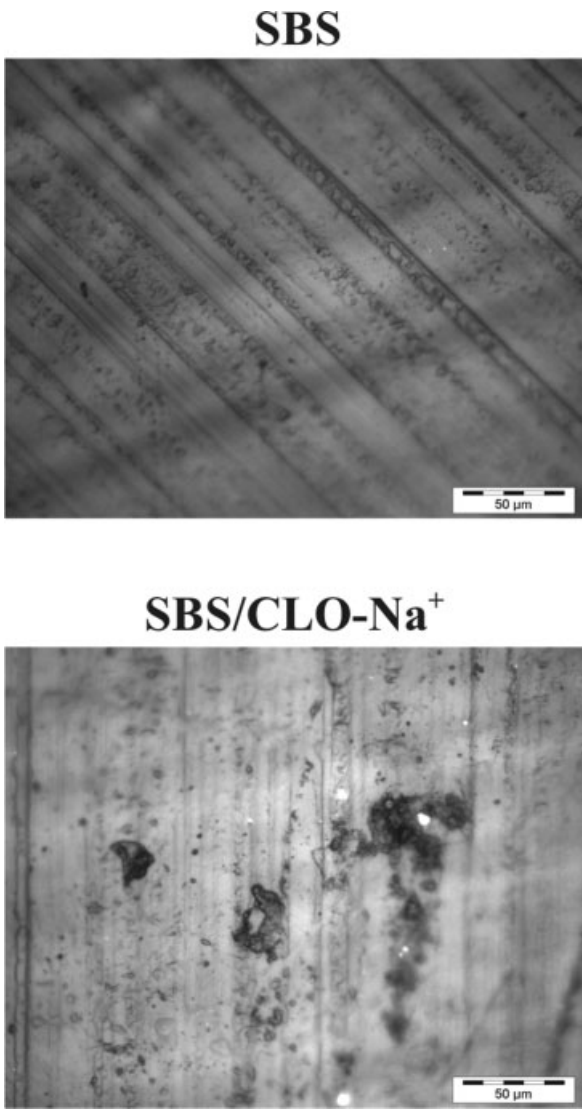

Figure 2 TOM micrographics of 100 μm thick films in transmission mode of SBS and SBS/CLO-Na^+ with 2 phr content.

dispersion of CLO-Na^+ in distilled water (10 wt %) was stirred vigorously overnight to get a good dispersion of the montmorillonite. Then modifier was added in excess and left under reflux with mechanical agitation. A white precipitate was obtained because the hydrophobic nature of the OMMT. It was then repeatedly washed with a 50/50 vol % ethanol/water hot mixture to remove the surfactant excess physisorbed around the tactoids and to eliminate the anion of the salt. Finally, it was dried at 80°C in a vacuum oven for 2 days to remove excess moisture. The OMMT designations are CLO-DMOcA for montmorillonite modification with DMOcA and CLO-BDHA for BDHA, respectively.

Preparation of SBS/OMMT nanocomposites

Nanocomposites were prepared by solving[21,32,33,35,44–48] several amounts of finely ground organo-montmorillonites and block copolymer in toluene at room temperature followed by dispersion in a sonication bath for about 6 h.[45] After that, the homogenous solutions were dried extensively at room temperature into Petri plates and subsequently annealed at 110°C in a vacuum oven for 3 h to remove any remaining solvent. Four SBS/OMMT hybrids with 1, 2, 5, and 10 phr OMMT were prepared with each OMMT (CLO-DMOcA and CLO-BDHA) and one with 2 phr of CLO-Na^+. Pristine SBS sample was also prepared following the same treatment (solution, sonication, and evaporation).

Characterization

FTIR analyses were performed in a Perkin–Elmer 16PC spectrometer. Nanocomposites were analyzed as solution-cast films from a 5 wt % toluene solution on KBr plates using the same KBr plate as background. Each spectrum was recorded over 36 scans,

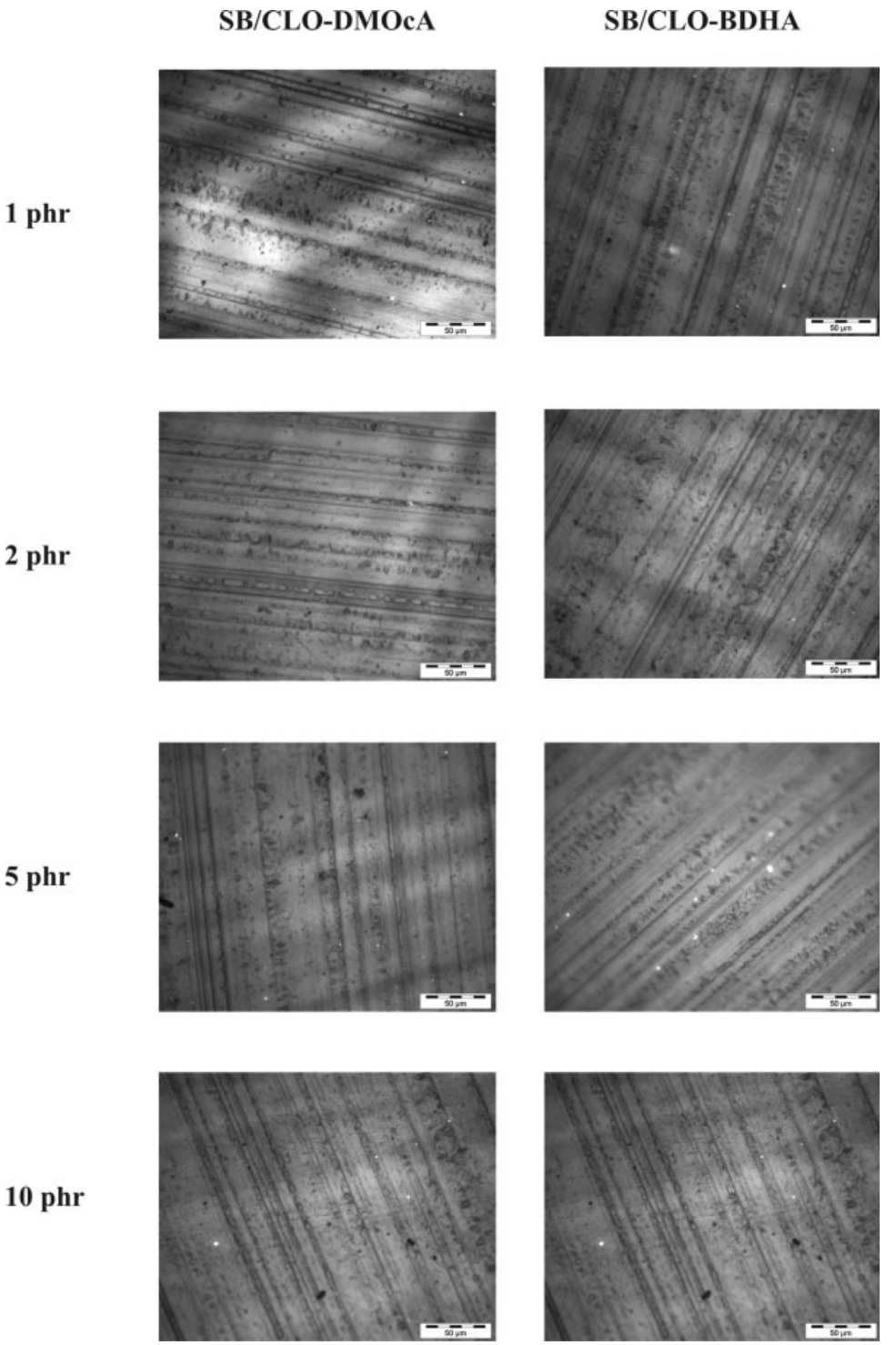

Figure 3 TOM micrographics of 100-μm thick films in transmission mode of nanocomposites with several OMMT contents.

in the range from 4000 to 400 cm^{-1} with a resolution of 8 cm^{-1}.

TGA analyses were performed using a Mettler Toledo TGA/SDTA851 in helium atmosphere at a heating rate of 10°C/min. Thermograms were recorded from room temperature to 1000°C. About 10 mg of compression-molded samples for nanocomposites measurements and fine dust samples for montmorillonites were used.

The intercalation of SBS into the galleries of OMMT and nanostructure patterns of block copolymer and nanocomposites was analyzed by WAXS and SAXS, respectively. WAXS and SAXS measurements were carried out in transmission geometry on

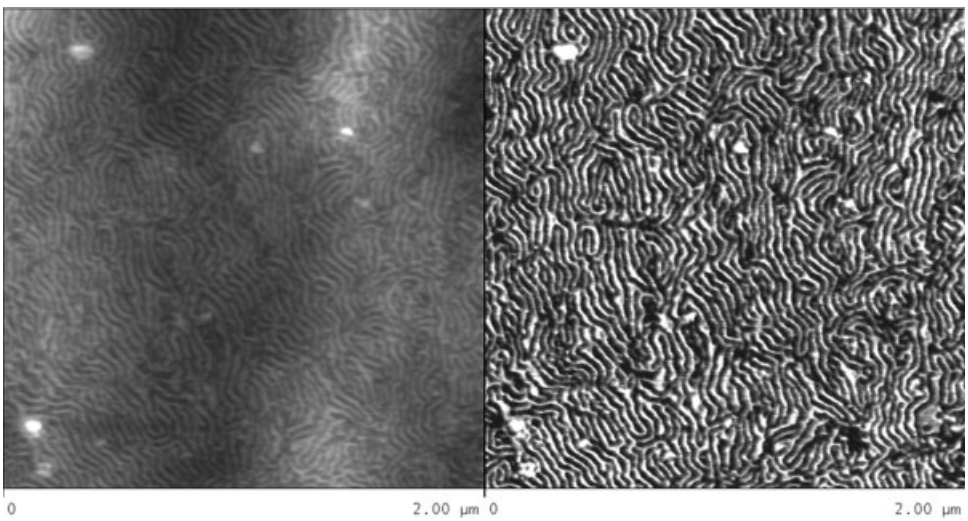

Figure 4 TM-AFM height (left) and phase (right) images for 1 mm thick SBS film annealed 3 h at 110°C.

a three-pinhole collimated system equipped with a Rigaku rotating anode (CuKα radiation $\lambda = 1.542$ Å, operating at 4.2 kW), an Osmic multilayer mirror for higher photon flux, and a MARCCD 2D detector (average pixel size 78.7 μm ×78.7 μm). The sample-to-detector distance was 1.8 m, and it was calibrated by using Ag-Behenate as standard. After the data collection, all patterns were background corrected and normalized with respect to thickness and, subsequently, were radially averaged yielding 1D SAXS patterns of $I(q)$ versus q, q being the scattering vector ($q = 4\pi \sin \theta/\lambda$, and 2θ being the diffraction angle). The Bragg spacing (D_s) was derived from the position of the first-order lattice scattering peak at q using the equation $D_s = 2\pi/q$. The software package Fit2D [http://www0.esrf.fr/computing/scientific/FIT2D/] was used to perform background subtractions, spatially correct the diffraction patterns, and calculate integrations of scattered intensity. The setup of the apparatus enabled a resolvable range of $0.05\ \text{nm}^{-1} \leq q \leq 7\ \text{nm}^{-1}$. All peaks appearing in the 1D pattern were subsequently fitted with Lorentzian

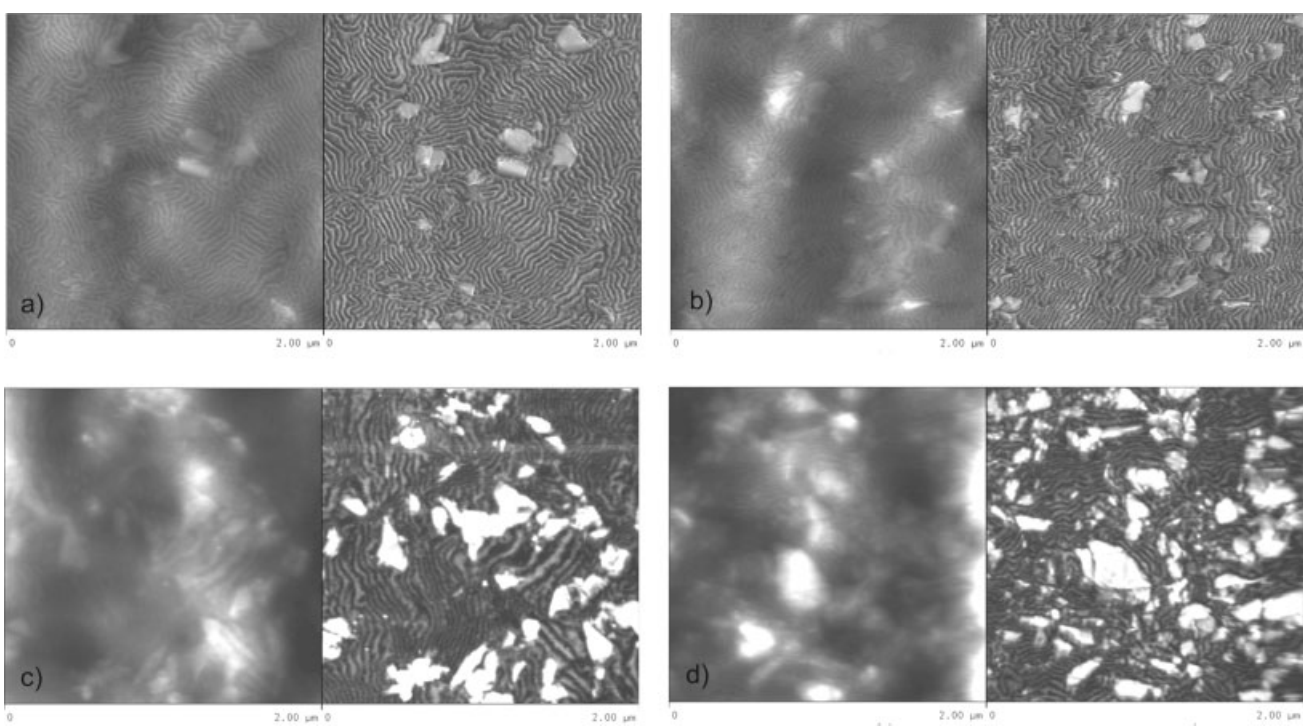

Figure 5 TM-AFM height (left) and phase (right) images for 1 mm thick SBS/CLO-DMOcA nanocomposites films annealed 3 h at 110°C. CLO-DMOcA content: (a) 1 phr, (b) 2 phr, (c) 5 phr, and (d) 10 phr.

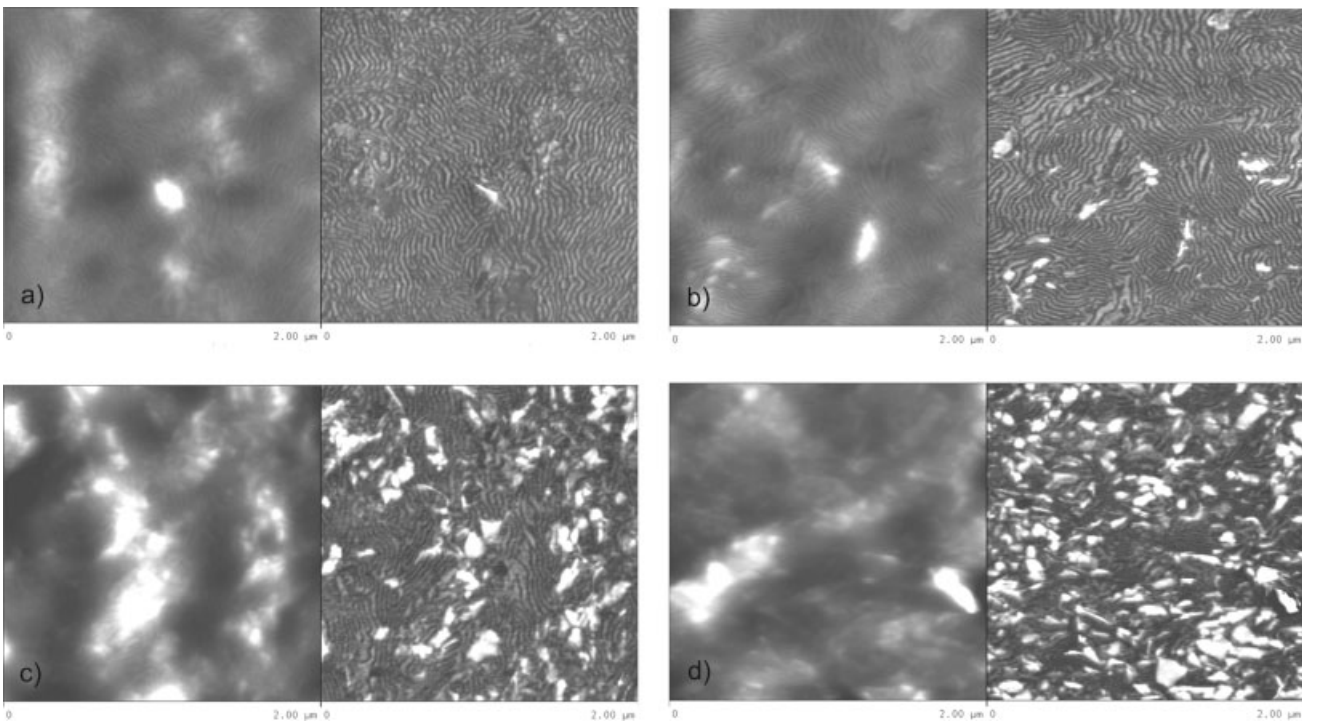

Figure 6 TM-AFM height (left) and phase (right) images for 1 mm thick SBS/CLO-BDHA nanocomposites films annealed 3 h at 110°C. CLO-BDHA content: (a) 1 phr, (b) 2 phr, (c) 5 phr, and (d) 10 phr.

functions by using Origin, and in the case of the weak reflections the Lorentz correction was also applied to the data. SBS and nanocomposite specimens with 1 mm thickness were obtained by cutting films prepared by press molding at 170°C. Before testing they were annealed for 3 h at 110°C.

The morphology of the specimens was studied by TOM, AFM, and TEM. Nikon Eclipse E600 microscope in transmission mode was used. A scanning probe microscope (Nanoscope IIIa, MultimodeTM from Digital Instruments) operating in tapping mode (TM-AFM) equipped with an integrated silicon tip/cantilever having a resonance frequency of 300 kHz from the same manufacturer was used. The height and phase images were obtained under ambient conditions with typical scan speeds of 1 line/s, using a scan head with a maximum range of 15 μm × 15 μm. The samples were parallelepipedic specimens of 1 mm thickness annealed for 3 h at 110°C. TEM micrographs were performed on a Tecnai G^2 20 TWIN CaB6 working at 200 kV. Electron transparent films of annealed samples for 3 h at 110°C were cryomicrotomed at −90°C using a diamond knife on a Leica Ultracut UCT and transferred to carbon film coated Cu grids. The specimens were stained by exposure for 20 h to osmium tetrooxide (OsO_4) vapor. As OsO_4 reacts preferentially with unsaturated carbon double bonds in the polybutadiene block, the stained polybutadiene phase appears dark in TEM micrographs.

RESULTS AND DISCUSSION

Figure 1 shows a comparative study of the optical transparency for all analyzed nanocomposites. All nanocomposites were transparent. TOM micrographs (Figs. 2 and 3) did not show soft agglomerates[49] in the organic hybrids (SBS/CLO-DMOcA and SBS/CLO-BDHA). On the contrary, SBS/CLO-Na^+ nanocomposite presented soft agglomerates higher than 40 μm size. To further investigate the morphology of SBS and nanocomposites, TM-AFM height and phase images of SBS, SBS/CLO-DMOcA, SBS/CLO-BDHA nanocomposites are shown in Figures 4–6. SBS copolymer was self-assembled into lamellar nanodomains with an interlamellar period of 32 nm. Figure 5(a,b) shows that structural perfection of SBS/CLO-DMOcA lamellae decreased with CLO-DMOcA content. Small aggregates of around 300–400 nm are also seen in the images. For 5 and 10 phr CLO-DMOcA contents, the increase of the amount of aggregates, but not their size, seemed to disturb more the formation of a perfect lamellar nanostructure, as shown in Figure 5(c,d) and also in SAXS profiles later. Figure 6(a–d) shows AFM images of nanocomposites containing CLO-BDHA. Lamellar structure perfection also decreased with increasing CLO-BDHA content. In addition, for 5 and 10 phr contents, a better dispersion than for the same contents of CLO-DMOcA was observed. AFM and TEM images, reported in Figures 7 and 8, indicate that for

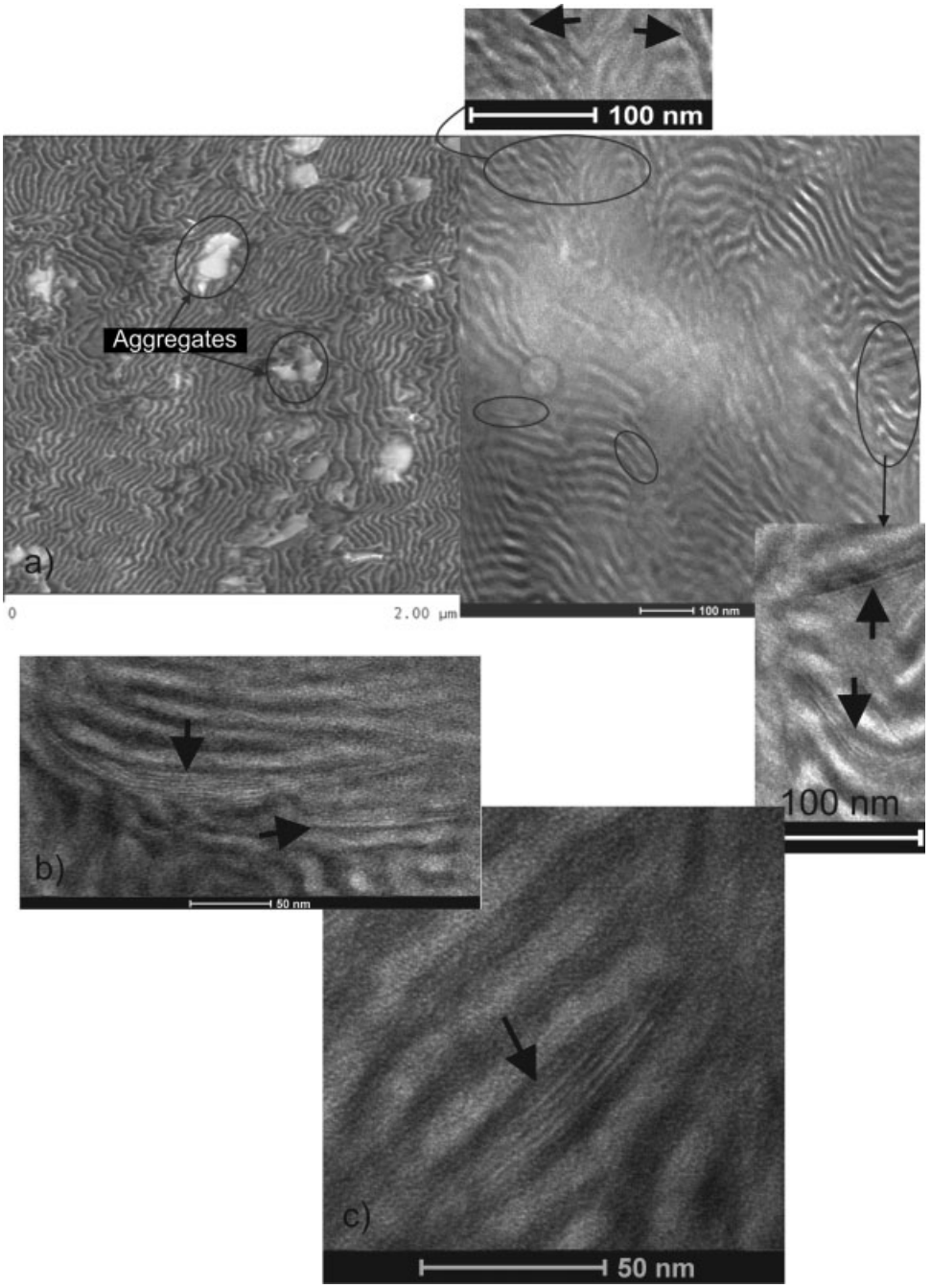

Figure 7 AFM-TEM comparative of SBS/CLO-DMOcA nanocomposite for 2 phr content: (a) TM-AFM phase (left) image and TEM (right) micrograph with several magnifications of the intercalated CLO-DMOcA layers. (b,c) Height-magnifications TEM micrographics of other zones showing intercalation.

both modified organic montmorillonites in some regions of bright lamellae of nanocomposites the lamellae seemed slightly broader than in the case of pristine SBS, about all in 2 phr OMMT samples. This fact seems to be related to the existence of intercalated OMMT lamellae inside the respective block compatible with the surfactant in the montmorillonite. In the case of CLO-DMOcA, these small intercalated tactoids into the polybutadiene (PB-block) lamellae [Fig. 7(a–c)] led to higher stiffness of PB microphase,[50] and consequently, these regions appeared brighter in AFM images. TEM micrograph shown in Figure 9 for an unstained nanocomposite containing 2 phr CLO-BDHA give more insights about the shape and dispersion of OMMT, again showing the presence of small aggregates.

Finally, as seen in Figure 10, TM-AFM phase and height images of a small area of SBS + 2 phr CLO-Na^+ show a higher extent of aggregation of the pristine montmorillonite than that existing for the SBS/

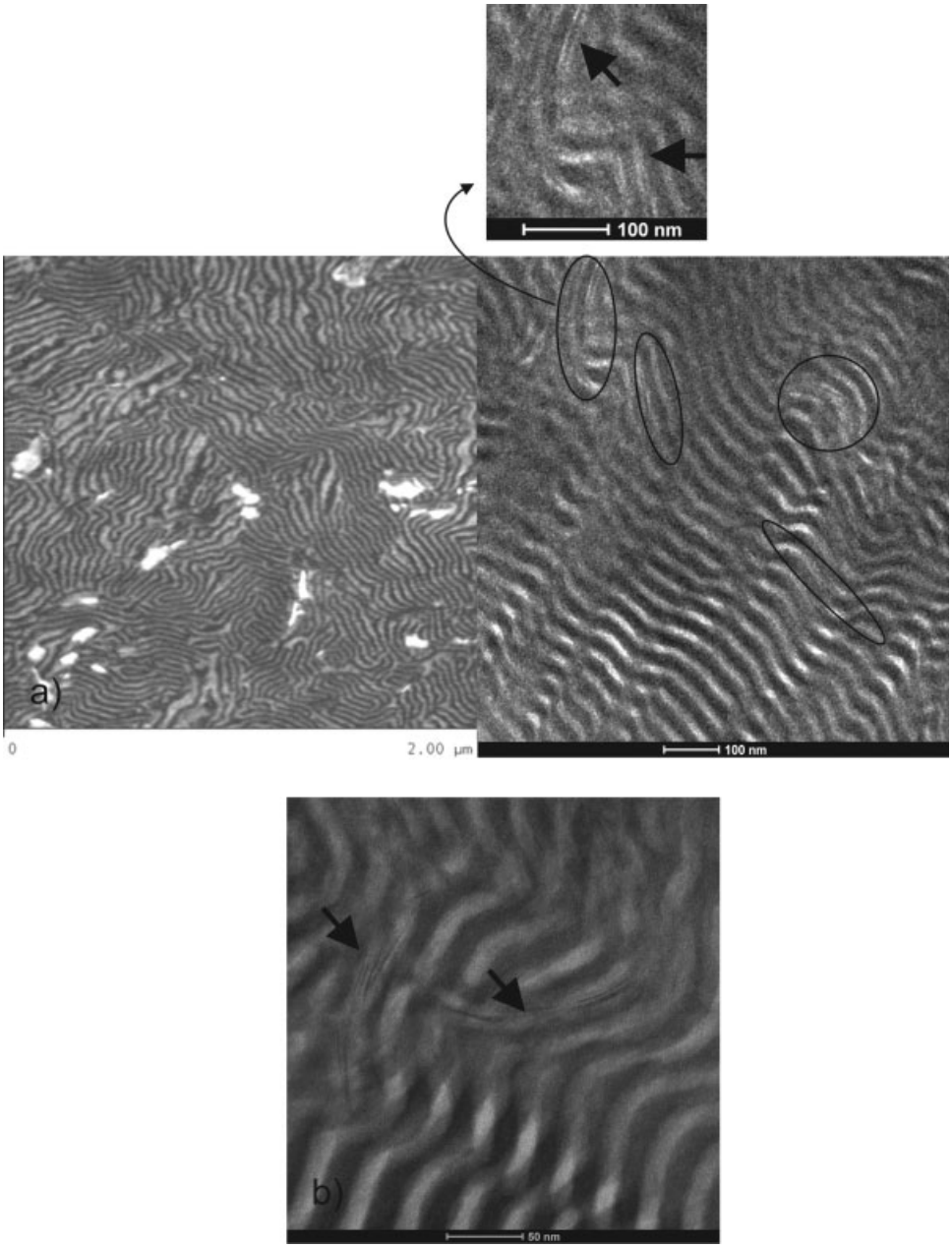

Figure 8 AFM-TEM comparative of SBS/CLO-BDHA nanocomposite for 2 phr content: (a) TM-AFM phase (left) image and TEM (right) micrograph with several magnifications of the intercalated CLO-BDHA layers and (b) Height-magnifications TEM micrographics of other zone showing intercalation.

OMMT nanocomposites, besides the rather poor dispersion that is shown earlier in TOM pictures.

X-ray diffraction spectra for CLO-DMOcA, SBS, and various representative hybrids are presented in Figure 11. The characteristic peaks and basal spacing were estimated by Bragg's equation [$d_{001} = \lambda/(2 \sin\theta)$]. CLO-DMOcA had a characteristic peak 2θ at 3.4° and also a residual peak at 7.2° of pristine CLO-Na^+ that corresponds to a basal spacing of 2.6 nm and 1.3 nm,[33] respectively. After CLO-DMOcA was added to SBS, a shift of the XRD peak to lower angles was observed, which implied an increase of the basal spacing to 4.0–4.2 nm. All nanocomposites with CLO-BDHA displayed a peak at 2θ equal to 2°, which corresponded to a *d*-spacing of 4.4 nm. This fact suggests a slightly higher affinity of SBS by the organic part of CLO-BDHA than for CLO-DMOcA. An increase of peak intensity by increasing the OMMT content in both types of nanocomposites was also observed. These characteristic peaks existing in all nanocomposites indicate that intercalated-montmorillonite nanocomposites were achieved.[32,34,35] The independence of the gallery height on silicate loading was consistent with results of Vaia and

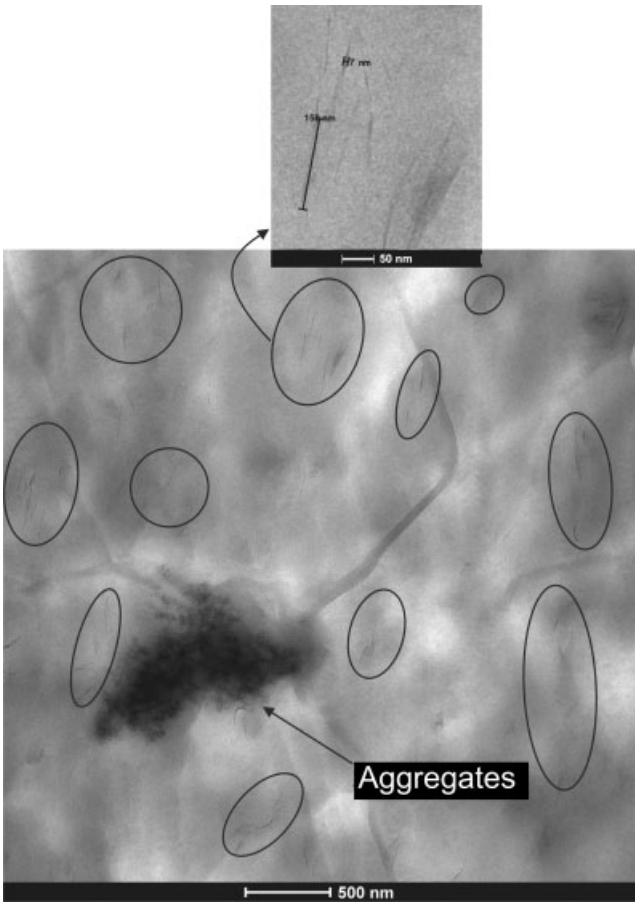

Figure 9 TEM micrograph for unstained 2 phr CLO-DMOcA content nanocomposite.

Giannelis for model PS-based nanocomposites[51] and Ren et al. for PI based nanocomposites.[44] Taking into account the microscopic images that are shown earlier, it becomes clear that XRD technique can provide no complete information about the real state of intercalation and dispersion on montmorillonites-based nanocomposites.

SAXS profiles of SBS and the nanocomposites with different CLO-DMOcA and CLO-BDHA contents and also the nanocomposite with 2 phr CLO-Na^+ are shown in Figure 12. The "q" peak positions of 1, 2, 3, and 4 (xq) peaks are characteristics of the lamellar morphology of the block copolymer. The interdomain spacing D_s is $\sim$ 31 nm, which corresponds to the width distribution of PS and PB lamellae. With the presence of CLO-DMOcA, the spacing slightly increased to 32 nm. These results agreed with AFM images. With CLO-DMOcA content, the more intense Bragg peaks became weaker and broader, and the peaks 2, 3, 4 (xq) nearly disappeared. This reveals that the addition of CLO-DMOcA reduced the structural perfection of the microphase-separated domain structure of the SBS.[32] The profiles of SBS/CLO-BDHA nanocomposites might suggest a larger affinity of the SBS by CLO-BDHA than by CLO-DMOcA as the OMMT layers disturbed the structure perfection to lesser extent, as shown in AFM images earlier. Moreover, the main Bragg peak shifted to values that corresponded to a spacing of 33–35 nm, suggests better miscibility of CLO-BDHA into PS nanodomains than that of CLO-DMOcA into PB ones, as shown by AFM earlier. For the same content, CLO-Na^+ also reduced slightly the structure perfection of the block copolymer but in a lower extent than for CLO-BDHA because the poor miscibility into the copolymer.

FTIR spectra of pristine CLO-Na^+, CLO-DMOcA and CLO-BDHA contained characteristic bands of montmorillonite and both surfactants are shown in Figure 13. Bands at 3640, 1045, 524, and 464 cm^{-1}

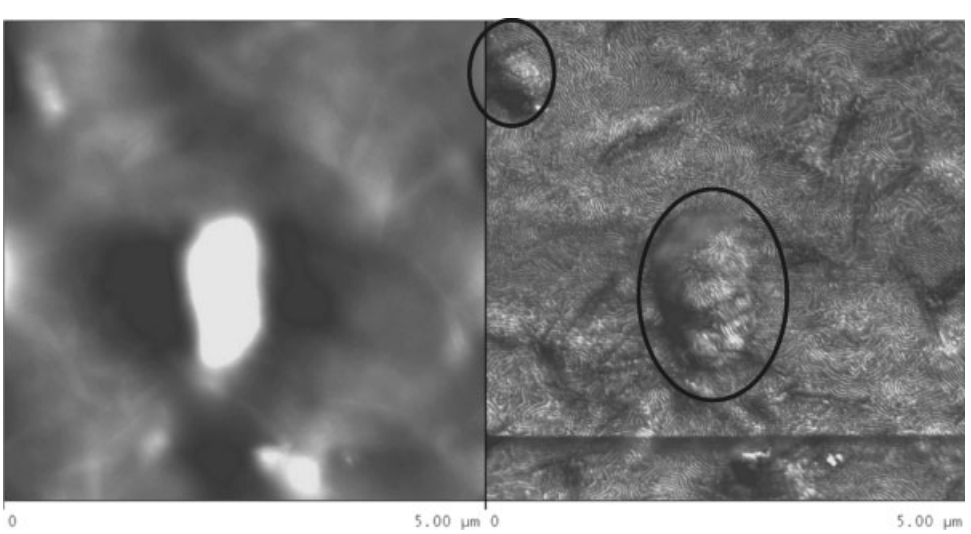

Figure 10 TM-AFM height (left) and phase (right) images for 1 mm thick SBS/CLO-Na^+ nanocomposite film annealed for 3 h at 110°C. Two phr CLO-Na^+ content.

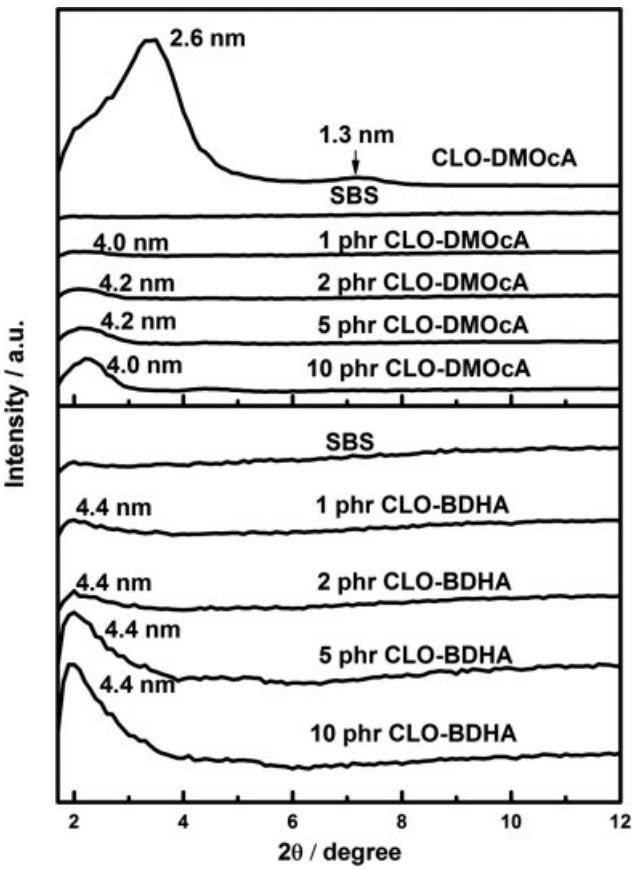

Figure 11 X-ray diffraction spectra for CLO-DMOcA, neat SBS, and nanocomposites with several CLO-DMOcA and CLO-BDHA contents.

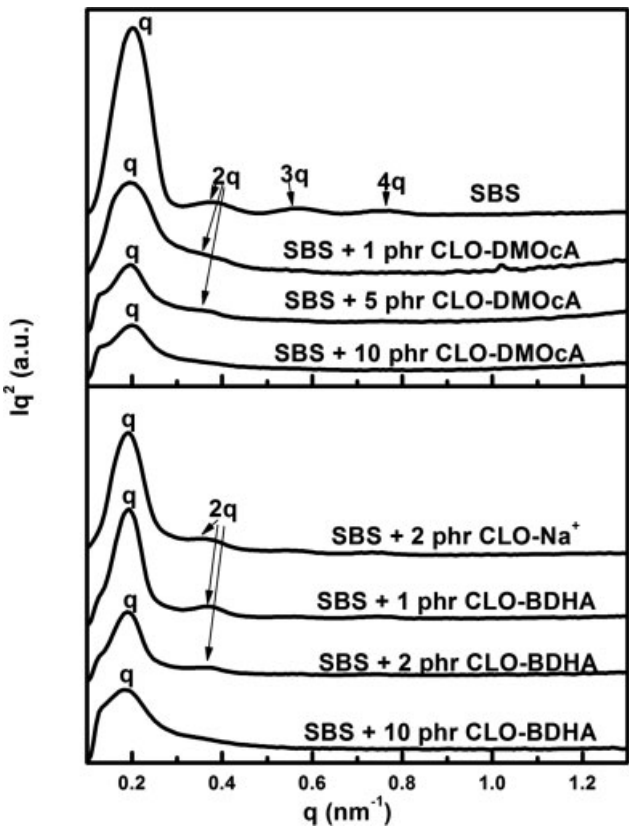

Figure 12 SAXS profiles for SBS and nanocomposites with several CLO-DMOcA and CLO-BDHA contents and nanocomposite with 2 phr CLO-Na^+.

are the typical bands of CLO-Na^+ attributed to the stretching vibrations of structural OH groups, the Si—O stretching vibrations and to Si—O—Al and Si—O—Si bending vibrations, respectively.[52,53] Peaks at 2925, 2854 cm^{-1} and that around 1467 cm^{-1} are the characteristic bands of symmetric and asymmetric stretching vibrations and bending vibration of methylene groups from DMOcA and BDHA, respectively. For pristine SBS (Figs. 14 and 15), all the bands reported in the literature were observed.[37] The existence of the montmorillonite into the nanocomposite was shown especially in 1100–1000 cm^{-1} and 600–400 cm^{-1} ranges. The presence of a doublet with two shoulders at 1045 and 1029 cm^{-1}, both increasing at higher montmorillonite content, was observed for all contents of SBS/CLO-DMOcA and SBS/CLO-BDHA nanocomposites. The shoulder at 1029 cm^{-1} originates from the contributions of both SBS and the montmorillonite. A similar behavior was also seen in the wave number region corresponding to Si—O—Al and Si—O—Si bending vibrations in which the peak of the copolymer at 539 cm^{-1} also contributed. SBS + 2 phr CLO-Na^+ did not show the shoulder at 1045 cm^{-1}, possibly as a consequence of the poor dispersion of the CLO-Na^+.

The derivative plot of thermal degradation (DTG) and thermal degradation weight loss (TG) of SBS and SBS/CLO-BDHA nanocomposites are shown in Figure 16. The decomposition of SBS occurred in two steps. In the first decomposition step, the loss was around 22 wt %, which mainly corresponds to 1,3-polybutadiene and 4-vinylcyclohexane from the

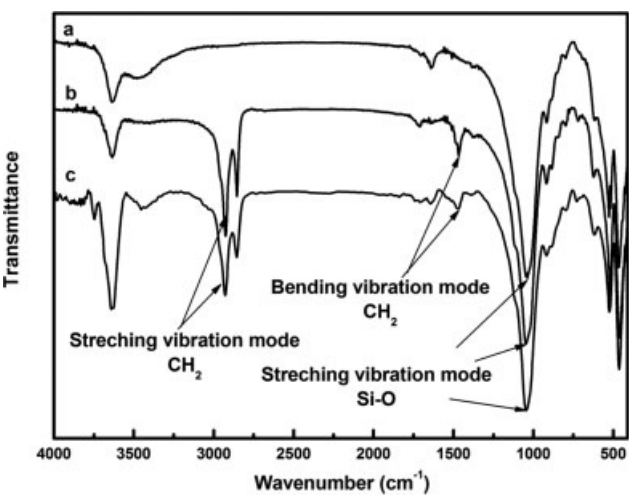

Figure 13 FTIR spectra for: (a) CLO-Na^+, (b) CLO-DMOcA, and (c) CLO-BDHA.

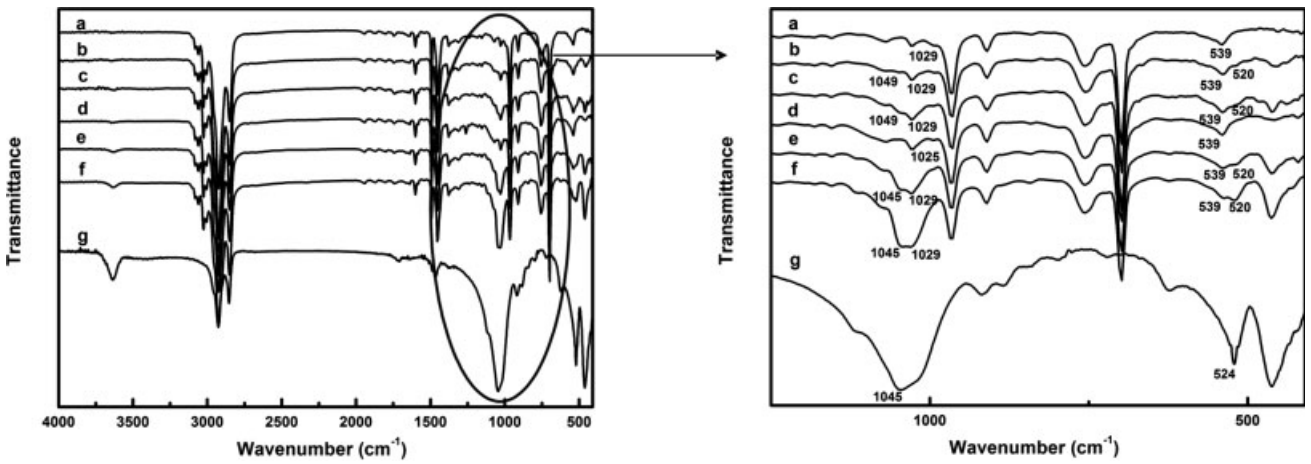

Figure 14 FTIR spectra for: (a) neat SBS and SBS/CLO-DMOcA nanocomposites with (b) 1 phr CLO-DMOcA, (c) 2 phr CLO-DMOcA, (d) 2 phr CLO-Na^+, (e) 5 phr CLO-DMOcA, (f) 10 phr CLO-DMOcA, and (g) CLO-DMOcA.

depolymerization reaction of 1,4-polybutadiene.[37] The second decomposition stage corresponds to the PS block.[37] The area of the peak of the first decomposition step (PB-block decomposition) increased with respect to pristine SBS for CLO-BDHA content up to 2 phr. On the contrary, for higher CLO-BDHA contents this trend was reversed. In the second decomposition step, (PS-block decomposition) the onset temperature of decomposition increased and the peak temperature shifted to higher temperatures as CLO-BDHA content increased up to 2 phr. Similar to PB-block decomposition, for higher CLO-BDHA contents this trend was reversed. The presence of small aggregates into PB-block could influence on the PB-block decomposition, although BDHA is selective to PS-block. At low contents, the increase of the area of PB-block decomposition might occur because the organic part of CLO-BDHA decomposed in this temperature range. As CLO-BDHA content increased up to 10 phr, the amount of aggregates into PB-block increased, reducing the area of decomposition of this block. On the other hand, in PS-block decomposition step, the presence of intercalated tactoids as well as small aggregates could give higher thermal stability to PS-block at low contents of CLO-BDHA than that for existing in SBS. This is possibly because the affinity between CLO-BDHA and PS block.[34] As the amount of agglomerates increased, the thermal stability of the PS-block decreased as shown by Nodera and Kanai[54] for polycarbonate-*block*-polydimethylsiloxane/silica nanocomposites.

Comparing both types of surfactants and CLO-Na^+ at 2 phr montmorillonite content, Figure 17, the PB-block decomposition step of the SBS/CLO-DMOcA presented two peaks at the same

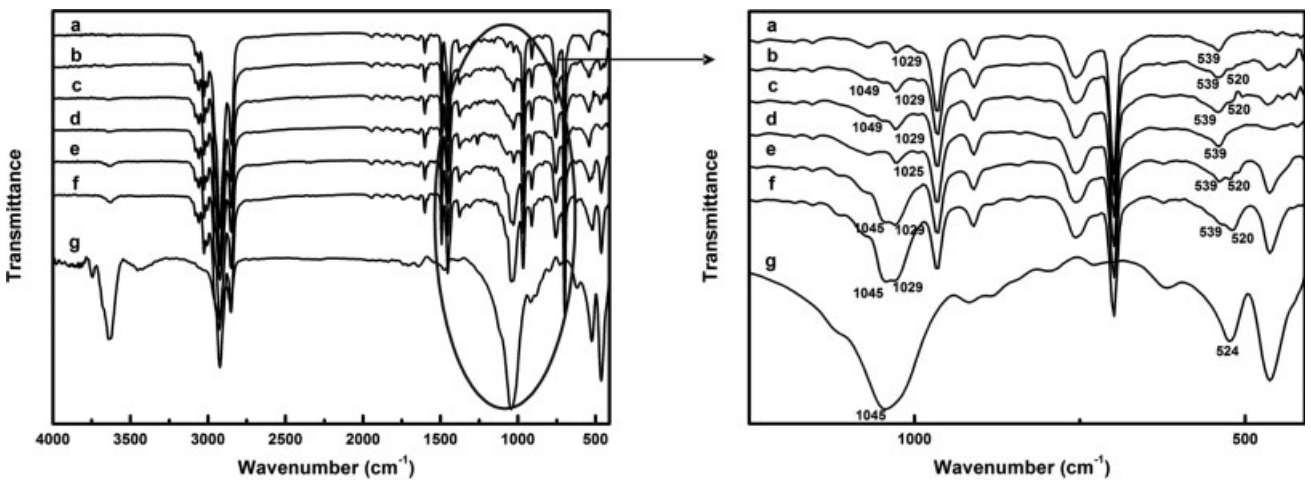

Figure 15 FTIR spectra for: (a) neat SBS and SBS/CLO-BDHA nanocomposites with (b) 1 phr CLO-BDHA, (c) 2 phr CLO-BDHA, (d) 2 phr CLO-Na^+, (e) 5 phr CLO-BDHA, (f) 10 phr CLO-BDHA, and (g) CLO-BDHA.

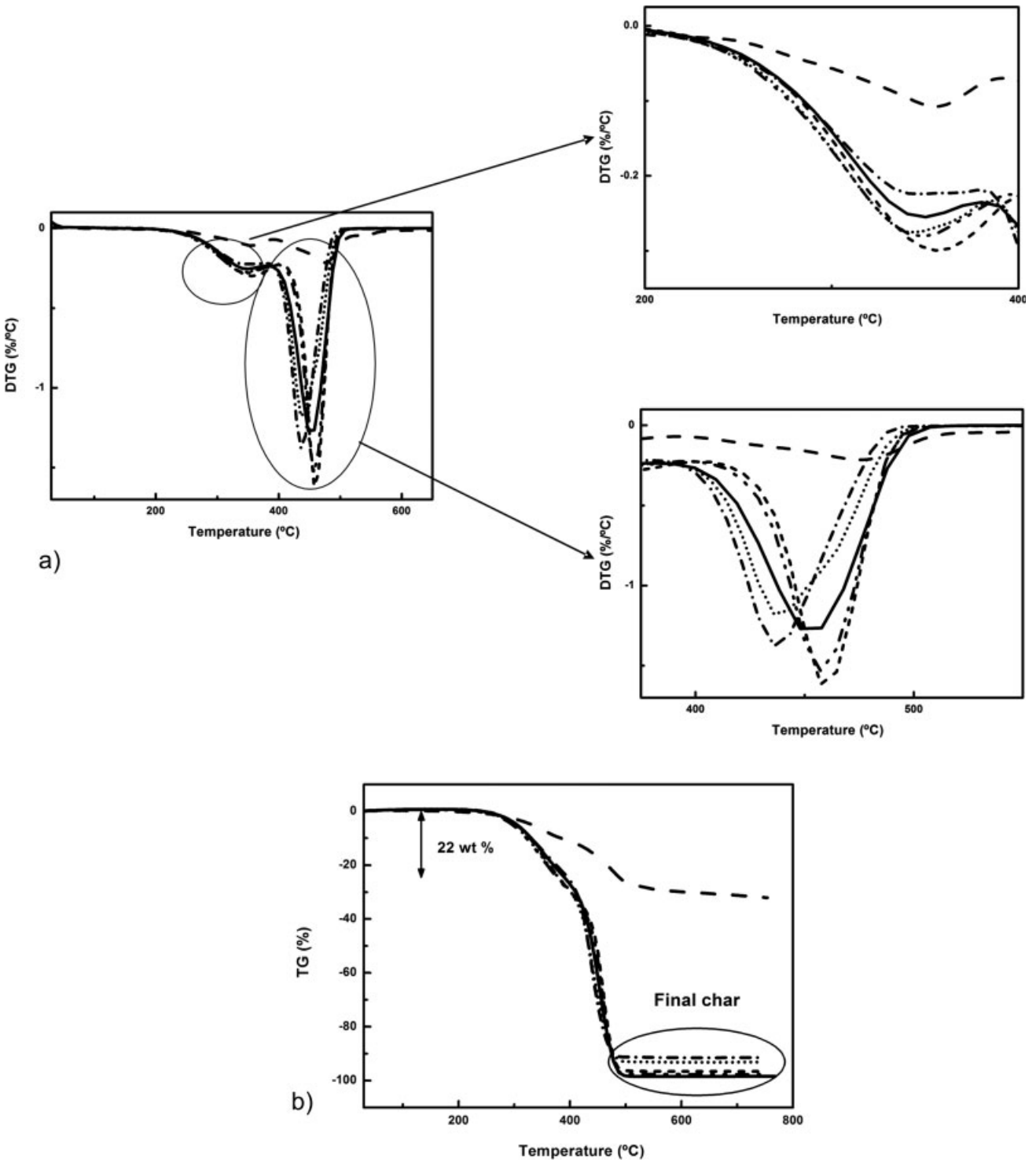

Figure 16 (a) DTG curves in several ranges and (b) TG thermograms for: neat SBS (—), neat CLO-BDHA (– –) and nanocomposites with 1 phr (–··), 2 phr (– – –), 5 phr (·····), 10 phr (–·–) CLO-BDHA.

temperature than pristine SBS (348°C) and another peak at 385°C. This suggests that intercalated tactoids into PB-block, as shown earlier in TEM micrographs, provided a higher thermal stability to PB block. In the case of SBS/CLO-BDHA, the peak shifted to a slightly higher temperature (355°C), but the decomposition was promoted by CLO-BDHA. In the PS-block decomposition step, the peak and onset of decomposition of SBS/CLO-BDHA shifted to slightly higher temperatures than for SBS. Low contents of CLO-DMOcA aggregates also increased the thermal stability of PS-block. CLO-Na^+ scarcely affected SBS decomposition because of its poor affinity with SBS.

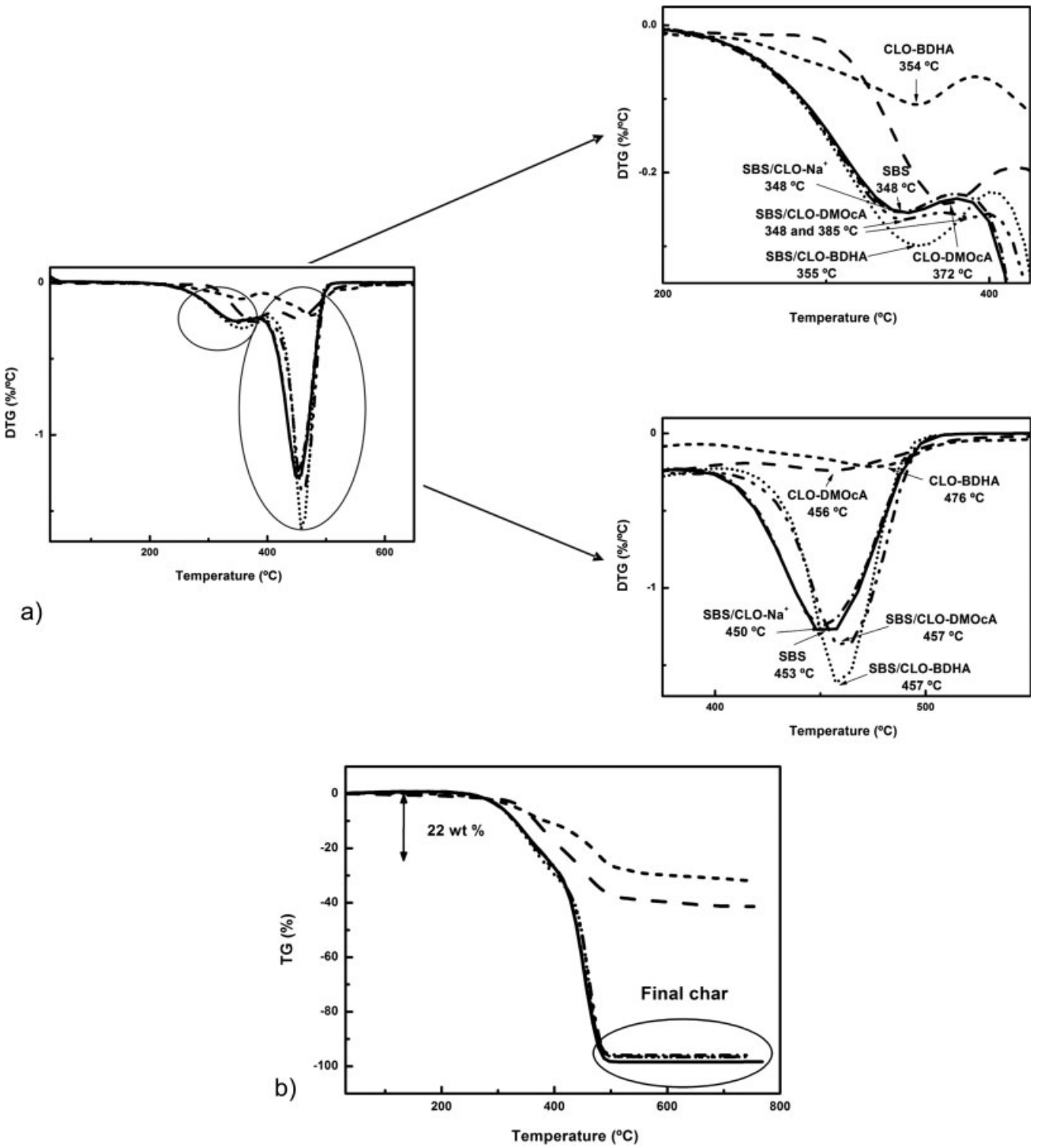

Figure 17 (a) DTG curves in several ranges and (b) TG thermograms for: neat SBS (—), neat CLO-DMOcA (– –), neat CLO-BDHA (– – –) and nanocomposites with 2 phr CLO-DMOcA (– ··), 2 phr CLO-BDHA (– – –), 2 phr CLO-Na^+ (– ·–).

CONCLUSIONS

A series of SBS block copolymer-matrix/OMMT and CLO-Na^+ nanocomposites were prepared by solvent casting. FTIR spectra provided information of the presence of the OMMT in the nanocomposites. The thermal stability of PB block and PS block was increased by the presence of intercalated tactoids of CLO-DMOcA and CLO-BDHA at low contents, respectively. X-ray spectra of SBS/OMMT demonstrated the intercalation of SBS into OMMT layers and proved the idea of a larger affinity of SBS by CLO-BDHA than for CLO-DMOcA. The type of surfactant seemed of capital importance to improve

dispersion of OMMT. Although SBS/CLO-DMOcA nanocomposites presented high-filler aggregation at CLO-DMOcA contents higher than 2 phr, those with CLO-BDHA showed better dispersion level and lower aggregation even at those contents, as shown in AFM images. Decrease of structure perfection of block copolymer and slightly increase of lamellae width by intercalated OMMT was demonstrated by SAXS profiles, AFM, and TEM images. TEM micrographs showed the predicted affinity of each OMMT for PS or PB blocks.

References

1. Jeon, H. S.; Rameshwaram, J. K.; Kim, G.; Weinkauf, D. H. Polymer 2003, 44, 5749.
2. Peanasky, J.; Cai, L. L.; Granick, S. Langmuir 1994, 10, 3874.
3. Anastasiadis, S. H.; Karatasos, K.; Vlachos, G. Phys Rev Lett 2000, 84, 915.
4. Usuki, A.; Kawasumi, M.; Kojima, Y.; Okada, A.; Kurauchi, T.; Kamigaito, O. J Mater Res 1993, 8, 1174.
5. Yano, K.; Usuki, A.; Okada, A.; Kurauchi, T.; Kamihaito, O. J. Polym Sci Part A: Polym Chem 1993, 31, 2493.
6. Messersmith, P. B.; Giannelis, E. P. J Polym Sci Part A: Polym Chem 1995, 33, 1047.
7. Wang, M. S.; Pinnavaia, T. J Chem Mater 1994, 6, 468.
8. Okamoto, M.; Morita, S.; Taguchi, H.; Kim, Y. H.; Kotaka, T.; Tateyama, H. Polymer 2000, 41, 3887.
9. Chen, G.; Qi, Z.; Shen, D. J Mater Res 2000, 15, 351.
10. Hilczer, B.; Kulek, J.; Markiewicz, E; Kosec, M. Ferroelectrics 2002, 267, 277.
11. Choi, H. J.; Kim, S. G.; Hyun, Y. H.; Jhon, M. S. Macromol Rapid Commun 2001, 22, 320.
12. Huang, X. Y.; Brittain, W. J Macromolecules 2001, 34, 3255.
13. Okamoto, M.; Nam, P. H.; Maiti, P.; Kotaka, T.; Hasegawa, N.; Usuki, A. Nano Lett 2001, 1, 295.
14. Ray, S. S.; Maiti, P.; Okamoto, M.; Yamada, K.; Ueda, K. Macromolecules 2002, 35, 3104.
15. Limary, R.; Swinnea, S.; Green, P. F. Macromolecules 2000, 33, 5227.
16. Krishnamoorti, R.; Silva, A. S.; Mitchell, C. A. J Chem Phys 2001, 115, 7175.
17. Silva, A. S.; Mitchell, C. A.; Tse, M. F.; Wang, H. C.; Krishnamoorti, R. J Chem Phys 2001, 115, 7166.
18. Castelletto, V.; Ansari, I. A.; Hamley, I. W. Macromolecules 2003, 36, 1694.
19. Lim, S. K.; Kim, J. W.; Chin, I.; Kwon, Y. K.; Choi, H. J Chem Mater 2002, 14, 1989.
20. Olayo-Valles, R.; Guo, S.; Lund, M. S.; Leighton, C.; Hillmyer, M. A. Macromolecules 2005, 38, 10101.
21. Lee, J. Y.; Park, M. S.; Yang, H. C.; Cho, K.;Kim J. K. Polymer 2003, 44, 1705.
22. Adhikari, R.; Michler, G. H.; Goerlitz, S.; Knoll, K. J Appl Polym Sci 2004, 92, 1208.
23. Leibler, L. Macromolecules 1980, 13, 1602.
24. Mayes, A. M.; Oliviera de la Cruz, M. J Chem Phys 1989, 91, 7228.
25. Mori, K.; Hasegawa, H.; Hashimoto, T. Polym J 1985, 17, 799.
26. Gehlsen, M. D.; Almdal, K.; Bates, F. S. Macromolecules 1992, 25, 939.
27. Barrat, J. L.; Fredrickson, G. H. J Chem Phys 1991, 95, 1281.
28. Vaidya, N. Y.; Han, C. D. Polymer 2002, 43, 3047.
29. Modi, M. A.; Krishnamoorti, R.; Tse, M. F.; Wang, H. C. Macromolecules 1999, 32, 4088.
30. Zhang, Y.; Wiesner, U. Macromol Chem Phys 1998, 199, 1771.
31. Zhao, J.; Morgan, A. B.; Harris, J. D. Polymer 2005, 46, 8641.
32. Lee, C. H.; Kim, H. B.; Lim, S. T.; Kim, H. S.; Kwon, Y. K.; Choi, H. J Macromol Chem Phys 2006, 207, 444.
33. Ha, Y.; Kwon, Y.; Breiner, T.; Chan, E. P.; Tzianetopoulou, T.; Cohen, R. E.; Óbice, M. C.; Thomas, E. L. Macromolecules 2005, 38, 5170.
34. Zhang, Z.; Zhang, L.; Li, Y.; Xu, H. J Appl Polym Sci 2006, 99, 2273.
35. Liao, M.; Zhu, J.; Xu, H.; Li, Y.; Shan, W. J Appl Polym Sci 2004, 92, 3430.
36. Yamaguchi, T.; Yamada, E. Polym Int 2006, 55, 662.
37. Serrano, E.; Zubeldia, A.; Larrañaga, M.; Remiro, P.; Mondragon, I. Polym Degrad Stab 2004, 83, 495.
38. Vazquez, A.; López, M.; Kortaberria, G.; Martín, L.; Mondragon, I. Appl Clay Sci 2008, 41, 24.
39. Van Krevelen, D. W. Properties of Polymers, 3rd ed. Amsterdam: Elsevier, 1990; Chapter 7.
40. Huang, J. C.; Zhu, Z. K.; Yin, J.; Qian, X. F.; Sun, Y. Y. Polymer 2001, 42, 873.
41. Lim, Y. T.; Park, O. O. Macromol Rapid Commun 2000, 21, 231.
42. Chen, T.; Zhu, J.; Li, B.; Guo, S.; Yuan, Z.; Sun, P.; Ding, D. Macromolecules 2005, 38, 4030.
43. Chen, G.; Kim, H.; Shim, J.; Yoon, J. Macromolecules 2005, 38, 3738.
44. Ren, J.; Silva, A. S.; Krishnamoorti, R. Macromolecules 2000, 33, 3739.
45. Há, Y. E. L.; Thomas, E. L. Macromolecules 2002, 35, 4419.
46. Morgan, A. B.; Harris, J. D. Polymer 2004, 45, 8695.
47. Watanabe, H.; Sato, T.; Osaki, K.; Yao, M.; Yamagishi, A. Macromolecules 1997, 30, 5877.
48. Mijovíc, J.; Lee, H.; Kenny, J.; Mays, J. Macromolecules 2006, 39, 2172.
49. Schaefer, D. W.; Justice, R. S. Macromolecules 2007, 40, 85.
50. Gutierrez, J.; Tercjak, A.; Garcia, I.; Peponi, L.; Mondragón, I. Nanotechnology 2008, 19, 155607/1–8.
51. Vaia, R. A.; Giannelis, E. P. Macromolecules 1997, 30, 7990.
52. Madejová, J. Spectrochim Acta Part A 1999, 55, 2467.
53. Madejová, J. Spectrochim Acta Part A 1998, 54, 1397.
54. Nodera, A.; Kanai, T. J Appl Polym Sci 2006, 101, 3862.